JOURNAL OF CATALYSIS **172,** 346–354 (1997)
ARTICLE NO. CA971875

Measurement of Gas Composition at the Center of a Porous Pellet during Adsorption and Catalytic Reaction under Dynamic Conditions

Andrew F. Cannestra, Laura C. Nett, and Richard K. Herz[1]

Department of Applied Mechanics and Engineering Sciences, University of California at San Diego, San Diego, California 92093-0411

Received October 18, 1996; revised August 18, 1997; accepted August 19, 1997

Gas composition is measured at the center of one-dimensional porous platinum/alumina pellets during carbon monoxide adsorption and catalytic oxidation. The apparatus is based on a single-pellet diffusion reactor that has been modified to allow continuous gas analysis and miniaturized in order to reduce the time constants of gas flow and mixing. Analysis of the CO adsorption response demonstrates that the centerplane volume and sample leak perturb the system only slightly and in a manner that can be accounted for during data analysis. A detailed kinetic model described previously is able to predict the qualitative features of the external concentration responses during carbon monoxide oxidation. However, the model is not able to predict major features of the responses measured at the pellet center, demostrating that the reactor is able to provide stricter tests of kinetic models than reactors in which only external compositions can be measured.

INTRODUCTION

Research in our laboratory is focused on the development of detailed kinetic models of reaction in porous catalysts. By "detailed kinetic model," we mean a model that describes adsorption and reaction events with rate equations representing elementary steps and, at the same time, describes transport processes within the porous material.

In previous work, we measured CO oxidation over a single pellet under steady-state and dynamic conditions (1) and performed numerical simulations of reaction and diffusion in the pellet using a detailed kinetic model (2). CO oxidation is important in emission control and is a model reaction whose behavior exhibits many important characteristics of surface reactions: competitive adsorption, adsorbate–adsorbate interactions, adsorbate islands, surface reconstruction, subsurface oxygen incorporation, structure sensitivity of some steps, nonlinear kinetics, and spatio-temporal pattern formation (3–9). Gulari *et al.* (10) recently reviewed CO oxidation behavior during dynamic operation over supported metal catalysts.

[1] To whom correspondence should be addressed. Fax: (619) 534-4543. E-mail: rherz@ucsd.edu.

We desire detailed kinetic models that are able to predict species concentrations under both steady-state and dynamic conditions. When only steady-state operation is considered, most kinetic models can be simplified by assuming that a single step is rate-determining such that an overall rate equation can be obtained easily. In addition, gradients caused by transport resistances often can be made negligible at steady-state, for example, by reducing the concentration of active sites, lowering the temperature, or reducing the size of catalyst particles.

The situation is more complex, however, when dynamic operation is considered. During dynamic operation, concentrations of species can span wide ranges such that no single step is rate-determining at all times. Concentration gradients within porous catalysts resulting from forced perturbations may take substantial time to decay as adsorbing species fill and empty surface sites. Values of the same diffusion coefficient determined by a steady-state method and by a dynamic method can differ substantially from each other (11, 12). In spite of the complexity of dynamic operation, such operation can have advantages in industrial processes (13–15) and can reveal important information about catalyst kinetics (11, 16–22).

In conventional adsorbers and reactors, species concentrations can be measured only in the bulk fluid flowing over the exterior surface of porous adsorbents and catalysts. Single-pellet reactors are useful in the study of detailed kinetics because interpellet gradients present within packed beds are eliminated. However, even when using a single pellet, external measurements may remain relatively insensitive to details of the adsorption or reaction system.

To see this, consider a case in which a gas adsorbs with a linear isotherm and a second case in which the gas adsorbs with a Langmuir isotherm that approaches saturation coverage at steady state. Although steady-state adsorption uptake measurements would be used to discriminate between the two models in practice, this system can serve as an example to illustrate a principle that also applies in the more complex situation of adsorption and reaction.

The simulated dynamic response of the gas flowing over the pellet exterior is shown for each example case in Fig. 1.

0021-9517/97 $25.00

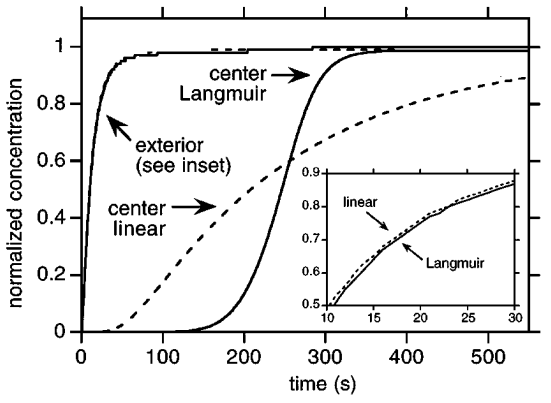

FIG. 1. Simulated concentration responses for gas adsorption with a linear (dashed lines) or Langmuir isotherm (solid lines). A one-dimensional pellet, 0.04 cm thick and 0.4 cm in diameter, is enclosed in a 0.56 cm^3 cell. The steady-state concentration of the adsorbing species is 3.8×10^{-8} mol/cm^3 and the gas enters the cell at rate of 0.05 cm^3/s and an exponential rise in inlet concentration of time constant 1.8 s. The effective diffusivity is 6.0×10^{-3} cm^2/s, the amount of gas adsorbed at steady state in both cases is 7.0×10^{-5} mol/cm^3 of pellet, and the Langmuir adsorption constant is 2.8×10^8 cm^3/mol.

Initially, all surface sites are empty and gas is fed to a mixing cell containing the pellet. At steady state, the adsorption uptake is the same in both cases. There is not a large difference between the two concentration responses, and the differences would be less apparent if errors and random scatter were present in these simulated data such as present in real data. In addition, there is no direct evidence of the extent of diffusion resistance and the presence of transient concentration gradients in the pellet.

For the two simulated experiments, the concentration responses present in the gas at the center of the pellet are also shown in Fig. 1. Whereas the responses over the pellet exterior are insensitive to the differences between the two cases, there is a dramatic difference in the concentration responses predicted at the pellet center: the gas with the linear isotherm penetrates rapidly to the pellet center and then rises gradually, whereas the gas with the Langmuir isotherm exhibits a delay before it penetrates to the center and then rises rapidly. The differences between the responses of the adsorbing species over the external surface of the pellet and the responses at the pellet center clearly indicate the presence of significant diffusion resistance in the pellet.

Since a mathematical model can be used to generate concentration profiles within porous pellets, an experimental system that would allow measurement of concentration responses at the interior of the porous material would facilitate development of models and discrimination between alternative models.

Such an experimental system for steady-state measurements was introduced by Roiter and coworkers (23, 24). This "single-pellet diffusion reactor" was further developed by Petersen and his students (25–28). Figure 2 shows a series of drawings which illustrate the concept of the single-pellet diffusion reactor and related single-pellet reactors. In the middle-left of the figure is an end view of a cylindrical tube containing a porous catalyst pellet. The series of three drawings from top to bottom on the right side of the figure are cross sections. In the cross sections, the rotational axes of the cylinders lie horizontally. When conditions are uniform radially over each face of the pellet, the pellet can be considered a one-dimensional system.

In the top cross section, a forced convective flow of gas ("bulk gas") is passed over both end faces of the pellet. When the two bulk gas streams have different compositions and there is no reaction occurring, this geometry is equivalent to that of Wicke–Kallenbach diffusion cells. In these cells, measurement of concentration differences across the pellet under nonreactive steady-state conditions allows determination of gas diffusion coefficients (12, 29). Dynamic experiments with this type of cell have been used by Dogu and Smith to determine values of diffusion coefficients and linear adsorption constants (30–32).

When the two bulk gas streams in the top cross section Fig. 2 have the same composition and there is catalytic

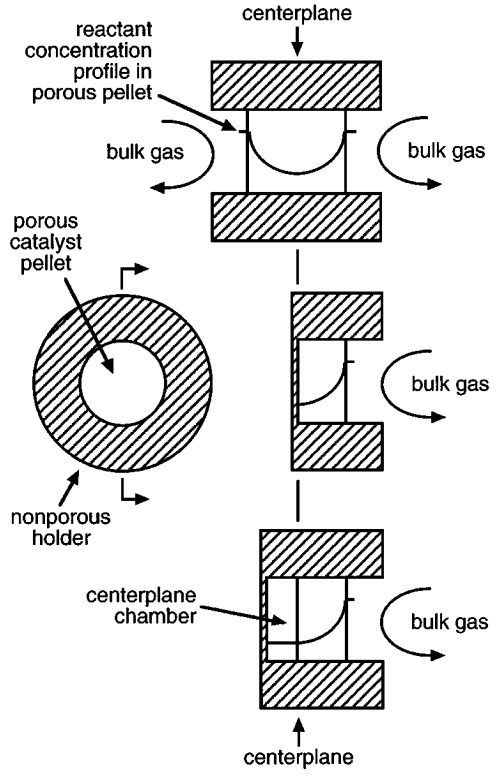

FIG. 2. Schematic diagrams illustrating the concept of a single-pellet diffusion reactor and related single-pellet reactors. (Middle, left) End view of a cylindrical pellet holder which contains a porous pellet. The series of three drawings (from top to bottom on the right) are cross sections of such a cylindrical holder and pellet.

reaction occurring in the pellet, the configuration is that of a one-dimensional single-pellet reactor. The general shape of the steady-state concentration profile of a reactant species inside the pellet is shown. Thin, disk-shaped pellets approach this one-dimensional geometry and have been used with infrared absorption spectroscopy to measure the total amount of species adsorbed on surfaces within the pellet during reaction (33–36). Information about the spatial distribution of adsorbed species has been possible only in the direction parellel to a pellet's face (37, 38). The related configuration of a reactor containing a single three-dimensional pellet has been used to study CO oxidation (39, 40) and liquid–gas processes important in liquid–gas trickle-bed reactors (41, 42).

The configuration represented by the top cross section in Fig. 2 is symmetrical about the pellet's centerplane, which is indicated by the vertical line running from the top to the bottom of the figure. At the centerplane, a zero-flux boundary condition exists. Because of the symmetry about the centerplane, the configuration shown in the middle-right of the figure is equivalent to the top configuration. In this middle configuration, the left side of this "half pellet," which lies along the centerplane line of the figure, is sealed by a nonporous plate. Gavriilidis and Varma (43) used this pellet geometry to study the selective catalytic oxidation of ethylene. Kopac *et al.* (44) used this geometry to study the reaction of SO_2 with activated soda under dynamic conditions. The "one-sided single-pellet" adsorption cell of Dogu *et al.* (45) has this pellet geometry and can be used to study diffusion and adsorption by measurement of external gas composition under dynamic conditions. Butt and his students (46–48) designed a reactor with this geometry in which the pellet is instrumented internally with thermocouples in order to measure internal temperature profiles and external gas composition during catalytic reaction.

Whereas single-pellet reactors with configurations equivalent to the top and middle cross sections in Fig. 2 are useful in studies of adsorption and catalyst kinetics, none allow verification of model predictions of gas composition inside the pellet.

The bottom configuration in Fig. 2 is that of the single-pellet diffusion reactor. It is similar to the middle configuration, with the difference that a "centerplane chamber" has been created on the left side of the pellet in order allow measurement of gas composition at the pellet centerplane. At steady state, the presence of this chamber does not alter the zero-flux boundary condition present at the centerplane side of the pellet. One method used to measure the centerplane composition in single-pellet diffusion reactors is infrared absorption spectroscopy (27). This method requires the use of large centerplane chamber volumes to allow for placement of windows and sufficient optical path length. Another method is gas chromatography (26, 28, 49). A sample of the gas in the centerplane chamber is withdrawn and injected into the GC. This procedure perturbs the system only briefly when sufficient centerplane chamber volume is provided. Values of both rate constants and effective diffusivity can be determined from measurement of reaction rate and bulk gas and centerplane composition (50). Au *et al.* (49) used a single-pellet diffusion reactor to study steady-state benzene hydrogenation over supported nickel. Suzuki and Smith (51) used a diffusion cell with this geometry and a thermal conductivity detector in the centerplane chamber to measure transient diffusion of nonadsorbing gases. Additional experiments involving transient H_2–D_2 exchange over unconsolidated particles supported on a wire screen were performed in this apparatus.

We have taken the concept of the single-pellet diffusion reactor and designed a version that allows adsorption and reaction to be studied under dynamic conditions. We call this design the "dynamic diffusion reactor" (52). Our objective is to measure the compositions of the bulk and centerplane gas under dynamic conditions where the bulk gas composition is being deliberately changed. Measurements in the centerplane chamber will approach those at the center of a "complete" pellet under dynamic conditions when (i) the centerplane chamber volume is well mixed, (ii) the time constant for filling and emptying the centerplane chamber with reactive species is small relative to the time constant of changes deliberately imposed on the bulk gas, and (iii) the rate at which gas is removed from the centerplane chamber is small relative to the rate at which reactant species can diffuse through the pellet.

The first two requirements are met in our design by the small dimensions of the centerplane chamber and high gas diffusion rates at low pressure. The third requirement is met by sampling the centerplane chamber with a continuous leak of gas withdrawn through a small pinhole in one wall of the chamber. The leaked gas is analyzed continuously by a mass spectrometer. The leak rate of gas can be made small such that the composition of the centerplane gas is perturbed only slightly by the leak.

EXPERIMENTAL

Figure 3 shows the reactor in cross section. The pellet holder is cross-hatched in this figure as in Fig. 2. The volume to the left of the pellet is the centerplane chamber; the volume to the right of the pellet is the bulk chamber through which reactants flow. The reactor components are made of stainless steel, except where noted below. The materials of construction had negligible activity in the work reported here.

Because of the toxicity of CO, the reactor and all other equipment associated with gas supply and handling are located inside of a walk-in fume hood. CO alarms are located outside of the hood near the operator's position.

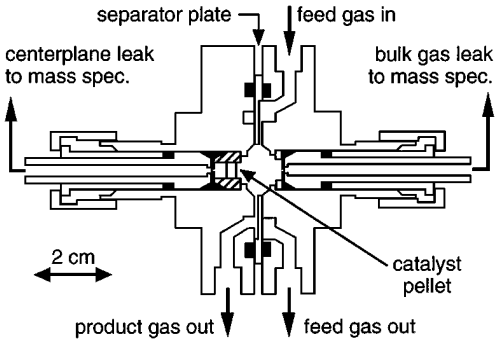

FIG. 3. Schematic of the reactor's cross section. The body of the reactor is generally rotationally symmetric about an axis running horizontally through the figure. The centerplane chamber is on the left side of the pellet. The bulk chamber, through which reactant gas flows, is on the right side of the pellet. The cross sections of the Viton O-ring seals are indicated by the solid black rectangles and triangles in the figure.

The seals are Viton O-rings. Five small-diameter O-rings seal the pellet holder and the two sampling tubes which protrude from each side of the reactor. Two large-diameter O-rings seal the two halves of the reactor against a copper separator plate. The cross-sections of the O-rings are represented by solid-black rectangles and triangles in Fig. 3.

A catalyst pellet is pressed from powdered Pt/Al_2O_3 directly into a stainless-steel pellet holder. The internal diameter of the pellet holder and, thus, the diameter of the pellets, is 0.4 cm. The thicknesses of the two pellets used in the work reported here were 0.051 and 0.064 cm. Pellets with active layers smaller than this thickness can be prepared by backing the active layer with an inert porous layer in order to provide mechanical support. Other physical forms of catalysts, in addition to pellets pressed from powder, can also be studied with this type of reactor. For example, a section of a preformed pellet or a catalytic membrane could be cut and cemented into a holder.

During assembly, the pellet holder is inserted into a socket in the left side of the reactor. After insertion of the pellet holder, the following are inserted; an O-ring, a washer, a stainless-steel foil with a laser-drilled "pinhole," another O-ring and, finally, one end of the sampling tube which leads to the mass spectrometer. The pinhole provides a leak of gas from the centerplane chamber to the mass spectrometer. A similar socket is located in the right half of the reactor. Into this socket, the following are inserted: a support ring, a washer, a stainless-steel foil with a pinhole, an O-ring and, finally, one end of the second sampling tube. The other end of each sampling tube is attached to a valve. The two valves are attached to a tee on the mass spectrometer chamber. Two separate experiments are required to measure the bulk and centerplane chamber compositions under one set of conditions.

The volume of the bulk chamber is 0.56 cm^3. The volume of the centerplane chamber in this design is determined by the internal diameter of the pellet holder and the distance between the centerplane side of the pellet and the opposite wall of the centerplane chamber in which the pinhole leak is located. In this work, the centerplane chamber volume was 0.044 cm^3.

Feed gas enters the right side of the reactor, flows around a circular distribution channel, and then out of the right side to a valve and pump. The gas distribution channel is formed by a circular groove in the right side of the reactor. A fraction of the feed stream can leave the gas distribution channel and enter the bulk chamber by flowing through eight radially spaced grooves machined in the right side of the separator plate. Gas leaving the bulk chamber, "product gas out," flows through a second set of grooves in the left side of the separator plate to a circular gas distribution channel in the left side of the reactor and then out to a valve and pump. The fraction of the feed stream that passes through the bulk chamber is controlled by the pressure differential between the feed and product gas distribution channels. Flow of gas through the small passages heats the gas to the pellet temperature before reaching the pellet.

A constant flow of gas can be supplied to the reactor through manual valves and tubing upstream of the reactor. Gas can also be injected into this tubing through a piezoelectric leak valve. Total gas pressures were measured by thermal heat-loss pressure gauges located near the feed gas outlet and product gas outlet ports. The pressures reported were determined using the average of the two gauge readings.

The gas flow fed to the reactor assembly in the experiments reported below was approximately 10 standard cm^3 per minute. Of this total flow, approximately 4% passes through the bulk chamber. The volumetric flow rate through the bulk chamber at a reaction pressure of 200 Pa would then be 3 cm^3 per second. The mean residence time for gas flow through the bulk chamber is then 0.2 s.

The experiments reported below were conducted with total gas pressures over the pellet of up to 350 Pa (1 Pa = 1 $N/m^2 = 10^{-5}$ atm $= 0.76 \times 10^{-2}$ Torr). Temperatures ranged from 125 to 175°C. At 100 Pa and 150°C, the mean free path of CO and O_2 is 10^{-2} cm, i.e., 100 μm. As a result, under the conditions used in this work, laminar and transitional gas flow occurred in the flow passages of the reactor, whereas molecular flow occurred in the pellet pores and through the pinhole leaks, which had diameters of 15 and 3 μm.

Gas in the bulk and centerplane chambers is mixed rapidly by diffusion. At 200 Pa and 150°C, the bulk diffusivity of CO in O_2 is 180 cm^2/s (53). Since the diameter of the bulk chamber is 1 cm and the diameter of the centerplane chamber is 0.4 cm, the time constants for diffusive mixing in the bulk and centerplane chambers are $\leq$6 ms. The time constant for diffusive mixing in the bulk chamber

is much less than the mean residence time of gas flowing through the chamber.

The time constant for filling and emptying the centerplane chamber with reactive species is determined by the ratio of the volume of the centerplane chamber and the rate at which reactant species can diffuse through the pellet. The rate at which reactant species can diffuse through the pellet is characterized by the conductance of the pellet, $D_e A_p/L_p$, where D_e is the effective gas diffusivity in the pellet, A_p is the geometric area of the pellet face, and L_p is the thickness of the pellet. Gas flow in the pellet pores is solely by Knudsen diffusion at the conditions of these experiments, even in the presence of a difference in total pressure across the pellet. The pellet conductance had a value of approximately 0.05 cm^3/s in this work, resulting in a time constant of 1 s for filling and emptying the centerplane chamber.

Because the flow from the pinhole leaks through the mass spectrometer chamber is by molecular flow, the time constant for flow of species through the chamber is dependent on the molecular weight of the species. The time constant for flow of CO through the measurement system is smaller than the time constant for flow of CO_2 by a factor equal to the square root of the ratio of their respective molecular weights, i.e., the time constant for CO is 80% of that for CO_2. Since the time constants for the response of the measurement system are about 0.1 s and the time scales of the dynamic experiments reported below range up to several hundred seconds, the differences in the response times of CO and CO_2 are too small to be seen in the figures shown here.

In all of the experiments shown, either Ar or Ne was present in the CO supply. The inert gas was used as an internal standard in the mass spectrometer measurements to correct for any changes in sensitivity between experiments. Production of CO_2 by reaction of CO and O_2 on the reactor walls and the mass spectrometer ionizer's filament was measured to be negligible in the experiments reported below, except where noted.

The CO pressures used here are 100 times lower than in studies of CO oxidation where large temporal and spatial variations in temperature caused by the heat of reaction have been observed (38, 54). As a result, temperature gradients across our pellets are negligible during both steady-state and dynamic experiments. The maximum temperature difference between a pellet's outer surface and its center can be estimated from $\Delta T_{max} = (-\Delta H) D_e C_{CO}/k_t$, where ΔH is the heat of reaction, C_{CO} is the CO concentration at the bulk face, and k_t is the effective thermal conductivity of the pellet (55). Using this equation, the temperature difference between the two faces of the pellet was less than 0.1 K under the conditions of the maximum steady-state rate observed in this work. With a fine thermocouple embedded in a pellet of similar dimensions under similar conditions, temperature changes of only ± 0.5 K were measured during periodic cycling of CO in O_2 in (1). The pellet in (1) was heated with a constant radiant flux from heating lamps and was suspended in ambient-temperature gas whose pressure was low and varied during the periodic cycling. Because of this, the small temperature variations measured in (1) were due primarily to changes in heat transfer rather than the heat of reaction and, thus, exceed any which may occur in the current reactor where the pellet, gas, and surrounding reactor body are at the same temperature.

RESULTS AND DISCUSSION

In initial work, large pinhole leaks were used in order to ensure sufficient signal. These pinholes were 15 μm in diameter in 13 μm-thick stainless-steel foil. With these pinholes, the leak rate from the centerplane chamber was significant with respect to the rate of gas diffusion through the pellet such that the steady-state gas pressure in the centerplane chamber was one-half the pressure in the bulk chamber. Experiments with these pinholes will be presented in order to illustrate important features of CO oxidation kinetics before experiments with small pinholes are described.

The results shown in Figs. 4–6 below were obtained using a 0.051 cm-thick pellet pressed from 12 mg of 2 wt% Pt/Al_2O_3. This is a sample of one of the catalyst materials ("chloride sample") whose preparation and characterization were described in Refs. (1, 2).

Figures 4 and 5 show results of an experiment in which CO was switched on and off periodically in a constant flow of O_2 at 150°C. The curves shown were obtained by averaging data from 20 periodic cycles that were recorded after the establishment of a steady cycling pattern. The O_2 pressure was 210 Pa and the maximum CO pressure was 85 Pa. CO oxidation over Pt exhibits a maximum in steady-state rate as CO pressure is increased at constant O_2 pressure (3–5, 56). The steady-state conditions with the CO flow on

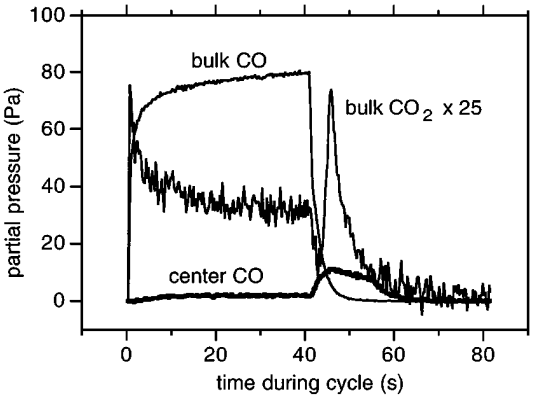

FIG. 4. Signals measured as CO was periodically turned on and off in a constant flow of O_2 over a Pt/Al_2O_3 pellet at 150°C. A single, averaged cycle is shown.

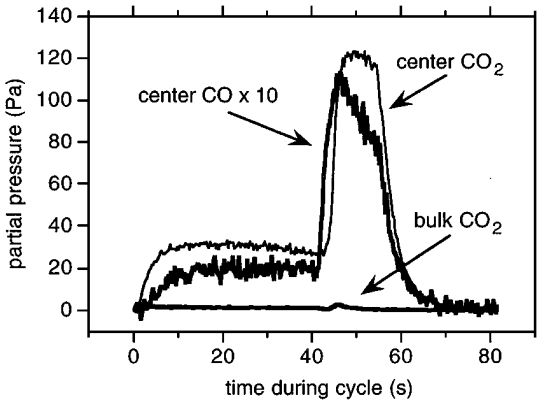

FIG. 5. Further results of the experiments shown in Fig. 4.

in Figs. 4 and 5 are slightly to the high-CO side of this rate maximum.

The bulk CO signal in Fig. 4 shows the increase of CO in the bulk chamber as CO is turned on at the start of a cycle and the decrease of CO as CO is turned off half way through the cycle period. The center CO signal remains low during the first half of the cycle because of the transient adsorption of CO and the conversion of CO to CO_2 by reaction. After CO is switched off in the feed gas, there is a period of time—approximately 45 to 65 s into a cycle—when the center CO pressure exceeds the bulk CO pressure and there is a net diffusive flux of CO from the centerplane to the bulk side of the pellet. This behavior occurs because CO, which had been adsorbed in the pellet during the first half of the cycle, desorbs into the gas phase as CO is pumped out of the reactor during the second half of the cycle.

The presence of reaction is indicated by the appearance of CO_2 in the bulk chamber in Fig. 4. The shape of the bulk CO_2 signal has the same qualitative features present in the signals measured in (1, 2) over the exterior of a single pellet of the same catalyst material in a standard reactor configuration. The first peak in CO_2 production at the start of a cycle is due to reaction of CO with adsorbed oxygen, which attained high coverages during the last half of the preceding cycle. The second peak in CO_2 production results primarily from reaction of adsorbed CO, which attained high coverages on some or all Pt particles during the first half of the cycle, with O_2, which can adsorb and react with adsorbed CO following the removal of the high CO pressures that maintained the high CO coverages. The feature most challenging to explain is the delay between the time the reactant CO is switched off and the time the second peak in CO_2 pressure starts to appear. This behavior can be explained by active sites with a bimodal distribution of CO adsorption strengths (2).

Figure 5 shows the bulk CO_2 signal along with the CO and CO_2 signals measured in the centerplane chamber. Note that the CO_2 pressure in the centerplane chamber greatly exceeds the CO_2 pressure in the bulk chamber. The centerplane CO_2 pressure remains constant just after the bulk CO is turned off and the bulk CO_2 pressure starts to decrease. Then the centerplane CO_2 pressure increases dramatically, with the leading edge of the peak in centerplane CO_2 pressure matching the appearance of the leading edge of the second peak in bulk CO_2 pressure. The centerplane O_2 signal, which is not shown, is essentially the mirror image of the centerplane CO_2 signal, with the reactant O_2 pressure decreasing as the product CO_2 pressure increases.

Following these experiments, we installed leaks that were 3-μm-diameter holes in 13-μm-thick stainless-steel foil. The conductance of these 3-μm pinholes is 1/60th of the conductance of the 15-μm pinholes. All results discussed below were obtained with the 3-μm pinholes.

Figure 6 shows the results of an experiment in which a flow of CO was periodically turned on and off over the same pellet used for the experiments in Figs. 4 and 5. There was no O_2 flow and only diffusion of CO and adsorption and desorption of CO occurred. The maximum pressure of CO was 220 Pa and the temperature of the system was 150°C. Data from one cycle out of a series of periodic cycles are shown in order to demonstrate that sufficient signal is obtained with the small leaks to get information without signal averaging. During the first half of the cycle, penetration of CO to the centerplane is delayed by the adsorption of CO on Pt. During the last half of the cycle, the CO pressure is higher in the centerplane chamber than the bulk chamber as CO desorbs from the Pt, diffuses out of the pellet, and is pumped from the bulk chamber.

The experimental responses were simulated by assuming that the local surface and gas concentrations were in equilibrium during the dynamic experiment and that the equilibrium is described by the Langmuir isotherm. The

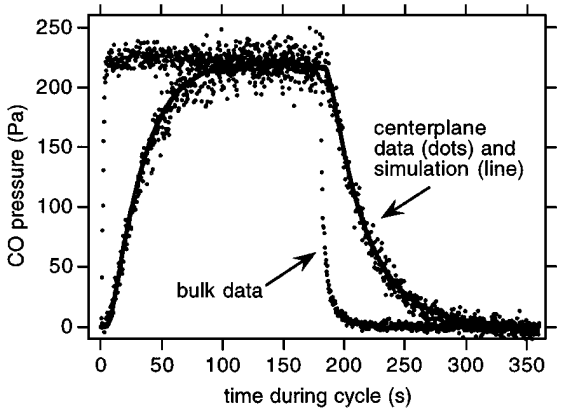

FIG. 6. The dots are experimental points measured during CO diffusion and adsorption in the Pt/Al_2O_3 pellet at 150°C with the 3-μm pinhole providing the sample leak. The curve is the centerplane response computed from a model of the experiment that includes a description of the centerplane volume and the sample leak.

assumption of close approach to local adsorption equilibrium was found to be reasonable in earlier studies of thermal desorption experiments (57) and in other simulations of these experiments in which this assumption was not made. The assumption of a simple Langmuir isotherm is an oversimplification for a supported Pt catalyst (58). However, we have found that transient adsorption–desorption experiments of this type appears to be insensitive to the detailed shape of the adsorption isotherm specified.

Under these assumptions, mole balances on [1] the gas-phase and adsorbed CO in the pellet, and [2] the CO gas in the centerplane chamber result in

$$\frac{\partial \Psi_p}{\partial t} = \frac{\left(1 + KC_{CO}^{max}\Psi_p\right)^2}{\varepsilon\left(1 + KC_{CO}^{max}\Psi_p\right)^2 + KC_s^{max}}\left(\frac{D_e}{L_p^2}\right)\frac{\partial^2 \Psi_p}{\partial \lambda^2} \quad [1]$$

$$\frac{d\Psi_c}{dt} = \left(\frac{D_e A_p}{V_c L_p}\right)\left.\frac{\partial \Psi_p}{\partial \lambda}\right|_{\lambda=0} - \left(\frac{S}{V_c}\right)\Psi_c, \quad [2]$$

where Ψ_p is the dimensionless gas concentration in the pellet's pores and Ψ_c is the dimensionless gas concentration in the centerplane chamber. The gas concentrations are normalized by the maximum gas concentration C_{CO}^{max}. K is the equilibrium adsorption constant, C_s^{max} is the maximum moles of CO that can adsorb per unit volume of pellet, and ε is the void fraction of the pellet. The dimensionless position inside the pellet of thickness L_p is specified by λ, with $\lambda = 0$ being the centerplane face of the pellet and $\lambda = 1$ being the bulk face of the pellet. V_c is the volume of the centerplane chamber, and S is the conductance of the pinhole leak to the mass spectrometer.

The first term on the right-hand-side of Eq. [2] is proportional to the rate of diffusion of CO out of the pellet and into the centerplane chamber. The seond term on the right-hand-side of Eq. [2] is proportional to the rate of flow of CO out of the centerplane chamber through the 3-μm pinhole. The conductance of the pinhole for CO at 150°C was calculated to be 2.2×10^{-4} cm^3/s, using relationships for molecular flow through a short tube (59).

For the boundary condition at the bulk face of the pellet, the dimensionless concentration in the pellet, $\Psi_p(1, t)$, is set equal to the dimensionless concentration measured experimentally in the bulk chamber, $\Psi_b(t)$. Signal-averaged data from several cycles are used for the bulk signal. For the boundary condition at the centerplane face of the pellet, the dimensionless concentration in the pellet is set equal to the dimensionless concentration calculated for the centerplane chamber:

$$\text{at the bulk face, } \lambda = 1\text{: } \Psi_p(1, t) = \Psi_b(t) \quad [3]$$

$$\text{at the centerplane face, } \lambda = 0\text{: } \Psi_p(0, t) = \Psi_c(t), \quad [4]$$

The effective diffusivity of CO during adsorption experiments at elevated temperatures was determined in two ways. We fit experimental data for CO diffusion during experiments at 30°C, where the surface was saturated with CO during the entire experiment and gas phase CO diffused in and out of the pellet as an inert gas would, and took the diffusion coefficient at this temperature and corrected it to the higher temperature using the square-root temperature dependence of Knudsen diffusion. We also fit experimental data for Ar and Ne diffusion during experiments at the elevated temperature and took the inert gas diffusion coefficients and corrected them to the value for CO diffusion by using the square-root dependence on molecular weight of Knudsen diffusion. Both methods give the same results for the effective diffusivity of CO. For the experiment shown in Fig. 6, $D_e = 4.7 \times 10^{-3}$ cm^2/s. Values of other parameters were $\varepsilon = 0.3$, $C_{CO}^{max} = 6 \times 10^{-8}$ mol/cm^3, and $C_s^{max} = 9 \times 10^{-5}$ mol/cm^3.

The solid curve in Fig. 6 is the response obtained by numerical integration of Eqs. [1] and [2] with boundary conditions given by Eqs. [3] and [4], i.e., the response obtained with the centerplane volume and leak present. The value of the adjustable parameter K for the curve shown was 1.2×10^6 cm^3/mol. Since we now have a model that describes the response obtained in this experiment, we can conduct a numerical experiment to determine the perturbations introduced by the centerplane chamber and the pinhole leak.

The solid curve in Fig. 7 is the same as the solid curve in Fig. 6. The dashed curve in Fig. 7 is the response that would have been obtained with zero centerplane volume and zero leak rate. To obtain this response curve, Eq. [2] was eliminated and Eq. [1] was integrated numerically, with Eq. [3] continuing to specify the boundary condition at the bulk face and a zero-flux boundary condition specified at

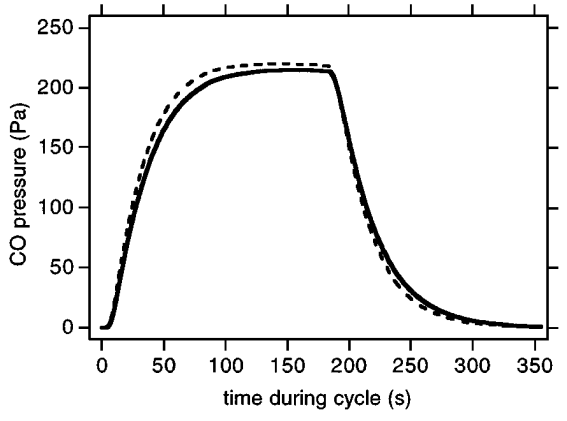

FIG. 7. The solid curve is the curve from Fig. 6. It is the simulated centerplane chamber response for CO diffusion and adsorption in the pellet, with the simulation including a description of the centerplane volume and the sample leak. The dashed curve is computed using the same parameter values and is the response that would be obtained with zero centerplane chamber volume and zero leak rate.

the centerplane face of the pellet:

$$\text{at the centerplane face, } \lambda = 0\text{: } \left.\frac{\partial \Psi_p}{\partial \lambda}\right|_{\lambda=0} = 0. \qquad [5]$$

The response with the zero-flux boundary condition is somewhat faster because of the absence of the centerplane volume and the need to fill it with CO. The response with the zero-flux boundary condition attains a higher level at the midpoint of the cycle because no CO is being leaked from the centerplane side of the pellet to the mass spectrometer. The leak reduces the steady-state signal level by 2%.

We conclude from Fig. 7 that the reactor provides a close approximation to diffusion and reaction in a single pellet, with the centerplane measurements closely representing the conditions present at the centerplane of a pellet where zero-flux conditions are present. Since the perturbations introduced by the centerplane volume and the leak can be accounted for, no approximations are required in the analysis of experimental data.

A new Pt/Al_2O_3, pellet, which was 0.064 cm thick, was installed in the reactor. This pellet had a significantly lower activity than the first pellet. Figure 8 shows the results of the CO oxidation experiments in which CO was periodically turned on and off in a constant flow of O_2. The average of seven periodic cycles is shown. The O_2 pressure was 92 Pa, the maximum CO pressure was 21 Pa, and the temperature was 175°C. Because of the low activity of the pellet, the flow rate through the reactor was reduced using a bypass line in order to obtain significant amounts of CO_2 on the bulk side of the pellet. This low flow rate produced a shape of the bulk CO signal that was distorted from the nearly square-wave signals normally imposed on the pellet. The bulk CO_2 signal level is about three times as high as the background signal produced in these measurements by reaction on the mass spectrometer's ionizer filament. These experiments show the concentration differences established between the bulk and centerplane sides of the pellet. Even with this low activity pellet, large concentration gradients were established in the pellet.

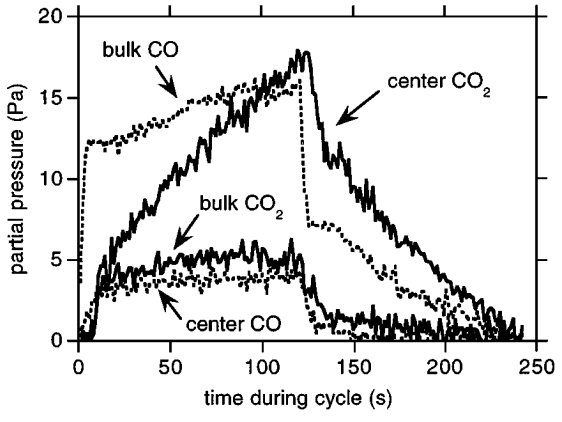

FIG. 8. Bulk and center responses for CO (dashed lines) and CO_2 (solid lines) measured during CO oxidation at 150°C over a second Pt/Al_2O_3 pellet.

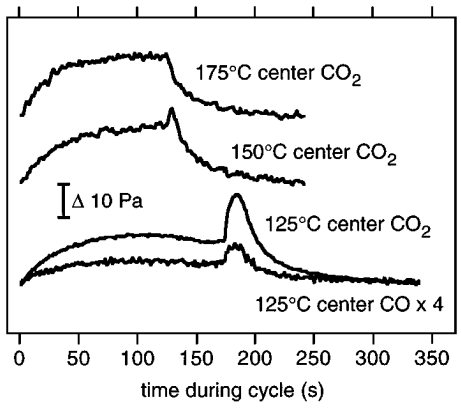

FIG. 9. Center responses measured during CO oxidation over Pt/Al_2O_3.

In these results, with the low activity pellet at 175°C, no peak in CO_2 production is observed after CO is turned off at the midpoint of the cycle, as it was in the experiments at 150°C with the higher activity pellet in Figs. 4 and 5. As the temperature was lowered with the low activity pellet, however, such a peak appeared in the centerplane CO_2 signal. The top curve in Fig. 9 shows reaction at the same temperature and same pellet but with a higher flow rate such that the signal imposed on the reactor again approximates a square wave. In Fig. 9, averages of seven periodic cycles are shown. The O_2 pressure was 110 Pa and the maximum CO pressure was 16 Pa. At 150°C a small peak in the CO_2 level appears just after CO is turned off at the midpoint of the cycle. At 125°C, there is a larger peak in centerplane CO_2 pressure. The appearance and growth of this CO_2 peak as the temperature is lowered is consistent with the interpretation that the peak is due to reaction of adsorbed CO that accumulates during the first half of each cycle. A longer cycle is presented at 125°C in order to show more clearly the appearance of a peak in centerplane CO pressure just after the midpoint of the cycle. This CO peak is further indication of the increased accumulation of adsorbed CO in the first half of the cycle at the lower temperature.

The detailed kinetic model developed in (2) is able to explain the qualitative features of the experimental bulk responses displayed in (2) and in Figs. 4 and 8 of this work. However, the model is not able to explain important aspects of the centerplane responses shown in Figs. 5 and 9. The model predicts a much smaller peak in center CO_2 than observed in this work. The model predicts a drop in center CO_2 just after the time when the bulk CO is switched off before the peak in center CO_2 appears but no such drop in center CO_2 was measured. Another discrepancy is that the model does not predict the peak in center CO that are shown in Figs. 5 and 9. These discrepancies are a

significant result of using the reactor since they demonstrate that measurements at the interior of a porous catalyst provide a more severe test of a kinetic model than external measurements alone. Further work is required to determine whether only adjustments in model parameter values are needed or whether additional processes have to be described in the model.

CONCLUSION

This work has demonstrated the ability to make gas concentration measurements at the interior of porous adsorbents and catalysts during adsorption and reaction under dynamic conditions. This ability provides direct measurement of any concentration gradients which may be present and provides strict tests of kinetic models.

ACKNOWLEDGMENT

Support for construction of the reactor was provided by the National Science Foundation under Grant CBT-8715427. L. Nett was a Patricia Harris Fellow.

REFERENCES

1. Racine, B. N., Sally, M. J., Wade, B., and Herz, R. K., *J. Catal.* **127**, 307 (1991).
2. Racine, B. N., and Herz, R. K., *J. Catal.* **137**, 158 (1992).
3. Herz, R. K., and Marin, S. P., *J. Catal.* **65**, 281 (1980).
4. Creighton, J. R., and White, J. M., *ACS Symp. Ser.* **178**, 33 (1982).
5. Engel, T., and Ertl, G., *Adv. Catal.* **28**, 1 (1979).
6. Mikhailov, A., and Ertl, G., *Chem. Phys. Lett.* **238**, 104 (1995).
7. Imbihl, R., and Ertl, G., *Chem. Rev.* **95**, 697 (1995).
8. Rotermund, H. H., Haas, G., Franz, R. U., Tromp, R. M., and Ertl, G., *Science* **270**, 608 (1995).
9. von Oertzen, A., Mikhailov, A., Rotermund, H. H., and Ertl, G., *Surf. Sci.* **350**, 259 (1996).
10. Gulari, E., Zhou, X., and Sze, C., *Catal. Today* **25**, 145 (1995).
11. Luss, D., *in* "Chemical Reactor Theory, A Review" (L. Lapidus and N. R. Amundson, Eds.), p. 191. Prentice Hall, New York, 1977.
12. Cui, L. C., Schweich, D., and Villermaux, J., *Chem. Eng. Process.* **26**, 121 (1989).
13. Zolotarskii, I. A., Bogdashev, S. M., and Matros, Y. S., *Kinet. Catal.* **30**, 1142 (1989).
14. Matros, Y. S., Bunimovich, G. A., and Noskov, A. S., *Catal. Today* **17**, 261 (1993).
15. Silveston, P. L., Hudgins, R. R., Bogdashev, S., Vernijakovskaja, N., and Matros, Y. S., *Chem. Eng. Sci.* **49**, 335 (1994).
16. Kobayashi, H., and Kobayashi, M., *Catal. Rev. Sci. Eng.* **10**, 139 (1974).
17. Bennett, C. O., *Catal. Rev. Sci. Eng.* **13**, 121 (1976).
18. Smith, J. M., *Stud. Surf. Sci. Catal.* **19**, 19 (1984).
19. Herz, R. K., and Sell, J. A., *J. Catal.* **94**, 166 (1985).
20. Razon, L. F., and Schmitz, R. A., *Chem. Eng. Sci.* **42**, 1005 (1987).
21. Siddal, J. H., Miller, M. L., and Delgass, W. N., *Chem. Eng. Commun.* **83**, 261 (1989).
22. Tamaru, K., *Catal. Sci. Technol.* **9**, 87 (1991).
23. Roiter, V. A., Korneichuk, G. P., Leperson, M. G., Stukanowskaia, N. A., and Tolchina, B. I., *Zhur. Fiz. Khim.* **24**, 459 (1950).
24. Korneichuk, G. P., Zhilailo, Ya. V., Roiter, V. A., and Garkavenko, I. P., *Zhur. Fiz. Khim.* **29**, 1073 (1955).
25. Balder, J. R., and Petersen, E. E., *J. Catal.* **11**, 195 (1968).
26. Balder, J. R., and Petersen, E. E., *J. Catal.* **11**, 202 (1968).
27. Hegedus, L. L., and Petersen, E. E., *Catal. Rev. Sci. Eng.* **9**, 245 (1974).
28. Wolf, E. E., and Petersen, E. E., *J. Catal.* **46**, 190 (1977).
29. Haynes, H. W., Jr., *Catal. Rev. Sci. Eng.* **30**, 563 (1988).
30. Dogu, G., and Smith, J. M., *AIChE J.* **21**, 58 (1975).
31. Dogu, G., and Smith, J. M., *Chem. Eng. Sci.* **31**, 123 (1976).
32. Burghardt, A., and Smith, J. M., *Chem. Eng. Sci.* **34**, 267 (1979).
33. Peri, J. B., *Catal. Sci. Technol.* **5**, 171 (1984).
34. Dwyer, S. M., and Bennett, C. O., *J. Catal.* **75**, 275 (1982).
35. Li, Y. E., Boecker, D., and Gonzalez, R. D., *J. Catal.* **110**, 319 (1988).
36. Sant, R., Wolf, E. E., *Chem. Eng. Sci.* **45**, 3137 (1990).
37. Kaul, D. J., and Wolf, E. E., *J. Catal.* **91**, 216 (1985).
38. Kaul, D. J., and Wolf, E. E., *J. Catal.* **93**, 321 (1985).
39. Onken, H. U., and Wicke, E., *Z. Phys. Chem.* **165**, 23 (1989).
40. Onken, H. U., and Wicke, E., *DECHEMA-Monogr.* **120**, 391 (1989).
41. Watson, P. C., and Harold, M. P., *AIChE J.* **39**, 989 (1993).
42. Hessari, F. A., and Bhatia, S. K., *Chem. Eng. Sci.* **51**, 1241 (1996).
43. Gavriilidis, A., and Varma, A., *AIChE J.* **38**, 291 (1992).
44. Kopac, T., Dogu, G., and Dogu, T., *Chem. Eng. Sci.* **51**, 2201 (1996).
45. Dogu, T., Yasyerli, N., McCoy, B. J., and Smith, J. M., *AIChE J.* **42**, 516 (1996).
46. Irving, J. P., and Butt, J. B., *Chem. Eng. Sci.* **22**, 1859 (1967).
47. Kehoe, J. P., and Butt, J. B., *AIChE J.* **18**, 347 (1972).
48. Butt, J. B., Downing, D. M., and Lee, J. W., *Ind. Eng. Chem. Fund.* **16**, 260 (1977).
49. Au, S. S., Dranoff, J. S., and Butt, J. B., *Chem. Eng. Sci.* **50**, 3801 (1995).
50. Herz, R. K., and Hegedus, L. L., *Chem. Eng. Sci.* **33**, 1561 (1978).
51. Suzuki, M., and Smith, J. M., *AIChE J.* **18**, 326 (1972).
52. Herz, R. K., Cannestra, A. F., and Racine, B. N., paper 49i, *in* "Am. Inst. Chem. Engrs. Natl. Mtg.," Miami Beach, Florida, Nov. 4, 1992.
53. Slattery, J. C., and Bird, R. B., *AIChE J.* **4**, 137 (1958).
54. Sant, R., and Wolf, E. E., *J. Catal.* **110**, 249 (1988).
55. Prater, C. D., *Chem. Eng. Sci.* **8**, 284 (1958).
56. Ertl, G., *Adv. Catal.* **37**, 213 (1991).
57. Herz, R. K., Kiela, J. B., and Marin, S. P., *J. Catal.* **73**, 66 (1982).
58. Guinn, K. V., Rhoades, D. S., and Herz, R. K., *Surf. Sci.* **393**, in press.
59. O'Hanlon, J. F., "A User's Guide to Vacuum Technology," 2nd ed. Wiley, New York, 1989.